LIMNOLOGY AND OCEANOGRAPHY
Letters

ASLO
Open Access

Limnology and Oceanography Letters 00, 2017, 00–00

doi: 10.1002/lol2.10043

LETTER

Phosphorus availability regulates intracellular nucleotides in marine eukaryotic phytoplankton

Elizabeth B. Kujawinski,[1]* *Krista Longnecker*,[1] *Harriet Alexander*,[2,3,a] *Sonya T. Dyhrman*,[2] *Cara L. Fiore*,[1,b] *Sheean T. Haley*,[2] *Winifred M. Johnson*[3]

[1]Department of Marine Chemistry and Geochemistry, Woods Hole Oceanographic Institution, Woods Hole, Massachusetts; [2]Department of Earth and Environmental Science and the Lamont-Doherty Earth Observatory, Columbia University, Palisades, New York; [3]MIT-WHOI Joint Program in Oceanography/Applied Ocean Science and Engineering, Cambridge, Massachusetts and Woods Hole, Massachusetts

Scientific Significance Statement

Phosphorus (P) is a central element in cellular metabolism that can limit primary production of eukaryotic phytoplankton in the ocean. Adaptation to low P is known to drive metabolic restructuring in eukaryotic phytoplankton, but the specific adaptive responses of cellular metabolites are poorly understood. Here we show that three model phytoplankton alter their metabolites under P deficiency, relative to P-replete conditions. We present evidence for a new model of P allocation within cells, where monophosphate nucleotides can act as a flexible P storage pool, allowing rapid and dynamic distribution of P to cellular processes.

Abstract

Marine eukaryotic phytoplankton adapt to low phosphorus (P) in the oceans through a variety of step-wise mechanisms including lipid substitution and decreased nucleic acid content. Here, we examined the impact of low P concentrations on intracellular metabolites whose abundances can be quickly adjusted by cellular regulation within laboratory cultures of three model phytoplankton and in field samples from the Atlantic and Pacific Oceans. We quantified the relative abundances of monophosphate nucleotides and their corresponding nucleosides, using a combination of targeted and untargeted metabolomics methods. Under P-deficient conditions, we observed a marked decrease in adenosine 5′-monophosphate (AMP) with a concomitant increase in adenosine. This shift occurred within all detected pairs of monophosphate nucleotides and nucleosides, and was consistent with previous work showing transcriptional changes in nucleotide synthesis and salvage under P-deficient conditions for model eukaryotes. In the field, we observed AMP-to-adenosine ratios that were similar to those in laboratory culture under P-deficient conditions.

*Correspondence: ekujawinski@whoi.edu

Author Contribution Statement: KL and EK designed and guided the lab and field metabolomics experiments. HA and SD contributed transcriptomics data, HA and KL linked the metabolomics and transcriptomics data. WJ and EK contributed the field data, CF and SH contributed culture data. EK, KL, and SD wrote the paper. All authors contributed editorial comments and approved the final version of the paper.

Data Availability Statement: Metabolomics data are available at MetaboLights (http://www.ebi.ac.uk/metabolights/) under accession numbers MTBLS154 (*Thalassiosira pseudonana*) and MTBLS295 (*Micromonas pusilla*). Transcriptome data are available at NCBI's Gene ExpressionOmnibus at GEO Series accession number GSE28134.

[a]Present address: Population Health and Reproduction, University of California – Davis, Davis, California
[b]Present address: Biology Department, Appalachian State University, Boone, North Carolina

Additional Supporting Information may be found in the online version of this article.

It is increasingly recognized that phosphorus (P) can limit primary production and carbon export, and shape phytoplankton community composition in the ocean (reviewed by Karl 2014). A number of strategies have been identified for mitigating the metabolic impacts of P deficiency in phytoplankton. These include increased scavenging from the surrounding environment through upregulation of inorganic P transporters and enzymes to access dissolved organic phosphorus (DOP; Ammerman and Azam 1985; Dyhrman et al. 2012) as well as structural changes such as the substitution of P-based lipids with sulfur-based lipids (Van Mooy et al. 2009; Martin et al. 2011). Many of these P deficiency responses show conservation across other functional groups of eukaryotic phytoplankton (reviewed by Dyhrman 2016).

Investigations to date have understandably focused on the largest intracellular P stores such as lipids, nucleic acids, and polyphosphate. However, the extent to which minor P stores are scavenged under low P is largely unknown (Karl 2014) but could prove important to maintenance of P homeostasis. For example, nucleotides carry up to three phosphate groups (e.g., adenosine 5′-mono-, di-, and triphosphate: AMP, ADP, and ATP, respectively), and play critical roles in cellular energy balances and phosphorylation capabilities. While it is reasonable to assume that phosphate-containing nucleotides would be subject to cleavage under P deficiency, few studies have explicitly examined the impact of low P on the dynamics of these critical metabolites. Instead, most studies have tacitly assumed that this pool is impervious to P deficiency due to its critical role in P homeostasis. However, similar investigations with nitrogen (N) deficiency have observed reduced concentrations of N-rich metabolites such as amino acids (Bromke et al. 2013) in N-deficient cultures of the centric diatom *Thalassiosira pseudonana*, concurrent with biochemical indicators of catabolism of the same amino acids (Hockin et al. 2012).

The overall metabolic response of an organism to nutrient limitation can be elucidated with metabolomics, or the study of molecules produced by a cell during metabolism and growth. These data provide unique insights into a cell's physiological state through the description and quantification of primary and secondary metabolites (Poulson-Ellestad et al. 2014). Yet, metabolic profiling studies under nutrient-limiting growth conditions are rare, relative to transcriptome or proteome investigations.

Metabolomics complements gene-based omics techniques by quantifying metabolic intermediates within active biochemical pathways. "Untargeted" metabolomics is used to describe, semi-quantitatively, all metabolites within a cell that can be detected with a chosen analytical method; thus it is appropriate for open-ended exploration of metabolic intermediates (Patti et al. 2012). In contrast, "targeted" metabolomics is used to quantify a pre-determined group of metabolites for precise cellular dynamics and assessment of relative rates of different metabolic pathways (Kido Soule et al. 2015). Metabolomics studies thus offer critical insights into cellular physiology that cannot be attained from other omics approaches.

In this study, we used untargeted and targeted metabolomics to examine the effect of low P on intracellular metabolites, in general, and on nucleotide abundances, specifically. We sought to understand how cells maintained critical P-dependent processes in the face of P deficiency. To answer this question, we quantified the relative abundances of intracellular nucleotides and nucleosides within three model phytoplankton and compared our laboratory-derived patterns to field observations.

Materials and methods

Overview

In this study, we cultured three phytoplankton—a diatom (*Thalassiosira pseudonana*), a prasinophyte (*Micromonas pusilla*), and a pelagophyte (*Aureococcus anophagefferens*)—under P-replete and P-deficient conditions. The chosen conditions facilitated comparison with published transcriptome and proteome data (Wurch et al. 2011*a*; Dyhrman et al. 2012; Whitney and Lomas 2016). We examined the relative abundances of intracellular monophosphate nucleotides (NMPs) and nucleosides in P-replete relative to P-deficient conditions. Metabolites observed in both targeted and untargeted methods showed similar trends across samples both within the diatom experiment (Supporting Information Fig. S1) and in complementary work (Johnson et al. 2016), facilitating comparisons across datasets. We then quantified particle-associated AMP and adenosine in field samples for comparison with our laboratory results. Detailed methods are provided in the Supporting Information.

Laboratory cultures

We cultured axenic *T. pseudonana* (CCMP 1335) in a modified L1 media with two phosphate conditions (Table 1) for two transfers prior to the start of this experiment, with a modified semi-continuous culturing method. The experiment contained two replicate cultures and one cell-free control for each treatment (12 flasks total for each treatment). We sampled one set of flasks destructively 0, 2, 8, and 10 days after inoculation. *T. pseudonana* cell abundances were calculated by converting the TOC concentrations using the value of 5.94 pg C cell^{-1} from Montagnes et al. (1994). The cultures were maintained under a 12 : 12 light : dark regime (84 μmol m^{-2} s^{-1}). We cultured axenic *M. pusilla* (CCMP 1545) under the same conditions as *T. pseudonana*. Samples for metabolomics were removed during exponential growth (day 6 in P-replete, day 4 in P-deficient) and at the onset of stationary growth (day 13 in P-replete and day 5 in P-deficient). We cultured axenic *A. anophagefferens* (CCMP 1984) in a modified L1 media, monitoring growth by relative fluorescence, and harvested cells for metabolite analyses at the onset of stationary phase. Growth conditions for the *T.*

Table 1. Overview of culture experiments.

	T. pseudonana		*M. pusilla*		*A. anophagefferens*	
	P-replete	**P-deficient**	**P-replete**	**P-deficient**	**P-replete**	**P-deficient**
Initial phosphate concentrations (μM)	36	0.4	36	0.4	36	0.4
Growth rate	0.5 day^{-1}	0.03 day^{-1}	0.46 day^{-1}	0.03 day^{-1}	0.47 day^{-1}	0.31 day^{-1}
Maximum cell yield	7.5×10^5 cells mL^{-1}	2.4×10^5 cells mL^{-1}	3.3×10^7 cells mL^{-1}	2.5×10^6 cells mL^{-1}	3.3×10^6 cells mL^{-1}	1.8×10^6 cells mL^{-1}
Maximum TOC concentration	1010 μM	278 μM	861 μM	309 μM	n.d.	n.d.
Number of significantly more abundant features*,†	462	121	n.d.	n.d.	n.d.	n.d.
Number of features (all time-points)‡	4979	4205	n.d.	n.d.	n.d.	n.d.

* Note that untargeted metabolic profiles were not analyzed for *M. pusilla* or *A. anophagefferens*.
† Using *p*-values adjusted for multiple comparisons allowing a False Discovery Rate of 10% (Storey and Tibshirani 2003).
‡ Sum of positive and negative ion modes.
n.d., not determined.

pseudonana transcriptome cultures are described in Dyhrman et al. (2012).

Metabolomics

For all laboratory samples, we captured cells on 0.2 μm Omnipore (Millipore) filters by gentle vacuum filtration, and extracted intracellular metabolites using a method modified from Rabinowitz and Kimball (2007). The extracts for targeted mass spectrometry analysis were dissolved in 95 : 5 (v/v) water : acetonitrile with deuterated biotin as an internal injection standard, and then analyzed with a C_{18} liquid chromatography (LC) column coupled to a Thermo Scientific TSQ Vantage Triple Stage Quadrupole Mass Spectrometer (Kido Soule et al. 2015). All reported concentrations are relative to an external calibration curve. We report fold changes and relative ratios wherever possible, i.e., when the denominator was not zero.

We desalted extracts for untargeted metabolomics prior to LC/MS analysis. We redissolved dried extracts in 0.01 M hydrochloric acid and re-extracted them using a 50 mg/1 cc PPL cartridge following the protocol of Dittmar et al. (2008). The resulting methanol extracts were dried, dissolved in 95 : 5 water : acetonitrile with deuterated biotin and analyzed in negative and positive ion modes with LC preseparation coupled to a 7-Tesla Fourier-transform ion cyclotron resonance mass spectrometer (FT-ICR MS). Parallel to the FT acquisition, we collected four data dependent fragmentation (MS/MS) scans at nominal mass resolution in the ion trap (LTQ). In this dataset, a mass spectral feature, or a putative metabolite, is defined as a unique combination of a mass-to-charge (*m/z*) ratio and a retention time along a LC gradient. Although untargeted metabolomics data are not fully quantitative, relative changes in feature (or metabolite) abundance can be discerned and statistically evaluated.

Comparison to previously published transcriptomes

We used the P-replete and P-deficient transcriptomes of *T. pseudonana* from Dyhrman et al. (2012) to survey the transcriptional responses related to purine and pyrimidine metabolism. We identified sequence tags with 100% identity to the *T. pseudonana* v3 genome (http://genome.jgi.doe.gov/Thaps3/Thaps3.home.html) (Armbrust et al. 2004) and assessed the statistical significance in differential expression of tags between P-replete and P-deficient conditions using Analysis of Sequence Counts (Wu et al. 2010). We predicted potential functionality of genes linked with metabolites with the Kyoto Encyclopedia of Genes and Genomes annotations from the *T. pseudonana* v3 genome. We manually searched targets of interest that were absent in the predicted pathways using BLASTX v2.2.27+ (e-value = 10 e –5) (Altschul et al. 1997). We then used Pathview (Luo and Brouwer 2013) to simultaneously plot the transcriptomics and metabolomics data on the biochemical pathways for *T. pseudonana*.

Field samples

Suspended particles from the Atlantic Ocean were collected in April and May 2013, from Uruguay to Barbados (38°S to 10°N). We collected water using Niskin bottles and filtered cells from 4 L onto pre-combusted GF/F glass-fiber filters (nominal pore size: 0.7 μm). Field samples from the Pacific Ocean (Line P) were collected in May 2012 in the same way except that cells from 2 L were filtered onto pre-combusted GF/A glass-fiber filters (nominal pore size: 1.6

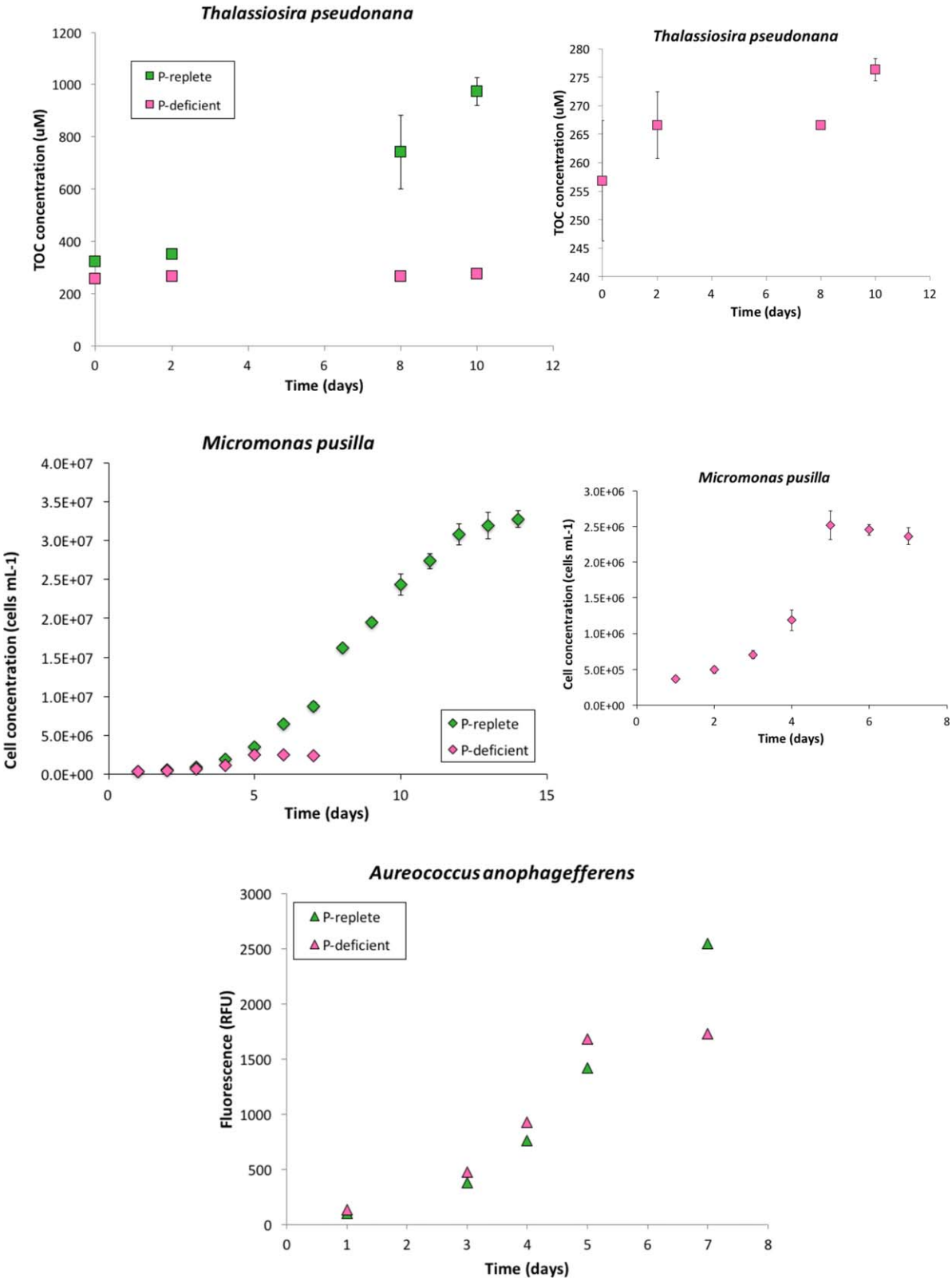

Fig. 1. Growth curves for *T. pseudonana* (top), *M. pusilla* (middle), and *A. anophagefferens* (bottom); for all, pink symbols represent P-deficient treatments and green symbols represent P-replete cultures. For *T. pseudonana*, growth was monitored using changes in total organic carbon concentrations; for *M. pusilla*, growth was monitored using cell counts; and for *A. anophagefferens*, growth was monitored using fluorescence. Insets are provided for the top two cultures to better visualize the low, but positive, growth. Metabolomics samples were collected on days 0, 2, 8, and 10 for *T. pseudonana*, on days 4 and 5 for P-deficient *M. pusilla*, on days 6 and 13 for P-replete *M. pusilla* and on day 7 for *A. anophagefferens*.

μm). We conducted procedural blanks for metabolomics analysis (using Milli-Q water) at the beginning and end of both field campaigns. We stored all filters at −80°C until extraction using the protocols described above. Salinities and fluorescence values are the average values (between 4.5 and 5.5 m) for each station collected on the downward CTD cast. Fluorescence values were then normalized to the highest value measured at these depths for the cruise.

Results

P deficiency affects growth rate and broad distribution of intracellular metabolites

In this study, we compared the metabolite response in three phytoplankton species under two P conditions, with the intention of imposing P deficiency with our lower P treatment. Consequently, we use the term "P deficiency" to conservatively describe any sample from a low-P treatment. In all cultures, P deficiency had a significant impact on phytoplankton growth (Table 1; Fig. 1). For *M. pusilla*, cell counts during the acclimation period confirmed growth under P deficiency (Supporting Information Fig. S2). We lack similar data for *T. pseudonana* but visual inspection of cultures showed growth prior to each transfer and carbon measurements during the experiment confirmed low, but positive, growth. However, these data cannot constrain whether *T. pseudonana* was in stationary or exponential growth at our different sampling points. In all three phytoplankton experiments, P deficiency affected the intracellular metabolite abundances across the targeted and untargeted metabolomics datasets (Table 1). We detected thousands of features at least once in the intracellular untargeted data from each treatment (Table 1), after blank correction. In the diatom culture, we detected the bulk of the features (4019) in both treatments, consistent with earlier metabolomics studies with these methods (Johnson et al. 2016) and expectations that intracellular features represent core metabolic pathways (Dettmer et al. 2007). After normalization to diatom biomass, 462 features exhibited significantly higher abundances at all time-points under P-replete conditions; similarly, 121 features exhibited significantly higher abundances under P-deficient conditions.

Nucleotide concentrations are affected by P deficiency

Of the significantly modulated features, we focused on intermediates within the purine and pyrimidine metabolic pathways (Supporting Information Table S1; Fig. S2). Combined, the targeted and untargeted metabolomics data revealed notable shifts between nucleosides and NMPs under the two growth conditions (Fig. 2). These molecules serve as precursors to the di- and tri-phosphorylated nucleotides (e.g., ADP, ATP; not measured in this study) and are the primary products of RNA degradation.

Under P-replete conditions, *T. pseudonana* contained detectable intracellular concentrations of nucleotides such as

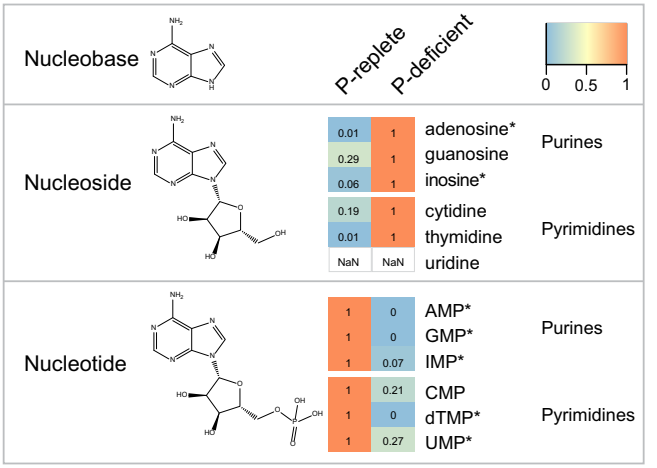

Fig. 2. Relative concentrations of nucleosides and nucleotides in phosphorus (P)-replete and P-deficient conditions for the diatom *T. pseudonana*. The average concentration across all sampling points for each treatment is presented after normalization to the maximum value of each metabolite across the sample set (numerical values in each block). This normalization enables the comparison of targeted and untargeted datasets. The color bar provides the scale used for the colors, where orange represents the maximum value and blue represents the minimum value. Example structures are provided for the nucleobase adenine, the nucleoside adenosine and the nucleotide, adenosine 5′-monophosphate (AMP). (*) indicates statistically significant differences between the two treatments. Individual data from each sampling point is available in Supporting Information Table S2.

AMP (Fig. 2; Supporting Information Fig. S3) and inosine 5′-monophosphate (IMP; Fig. 2). In contrast, we did not detect these P-containing molecules in the intracellular metabolite pool under P-deficient conditions. Instead, we observed elevated nucleosides at all time points under P deficiency. For example, adenosine and inosine were elevated and positively correlated to one another (Spearman's $r = 0.9076$, p-value $\ll 0.0001$). Similarly, the NMPs were correlated across the dataset (for AMP and IMP: Spearman's $r = 0.9166$, p-value $\ll 0.0001$). We observed a parallel pattern in the pyrimidine pathway (Supporting Information Fig. S2B), where the pyrimidine-based NMPs were all elevated relative to their nucleoside counterparts such as cytidine (Supporting Information Fig. S4) in P-replete *T. pseudonana* (Fig. 2). Not all nucleoside and NMP concentrations had statistically significant differences between treatments (Fig. 2), but all NMP-nucleoside pairs exhibited similar overall patterns across all time-points (Supporting Information Table S2). We estimated the minimum concentration of NMPs in a P-deficient cell would be 0.0005 amol, well below our detection limit (Supporting Information Calculation S1). Thus P-deficient cells in our experiments could reasonably contain the necessary, albeit undetectable, NMPs for nucleic acid synthesis during growth.

A conservative comparison between the *T. pseudonana* metabolic profiles and transcriptomes (Dyhrman et al. 2012)

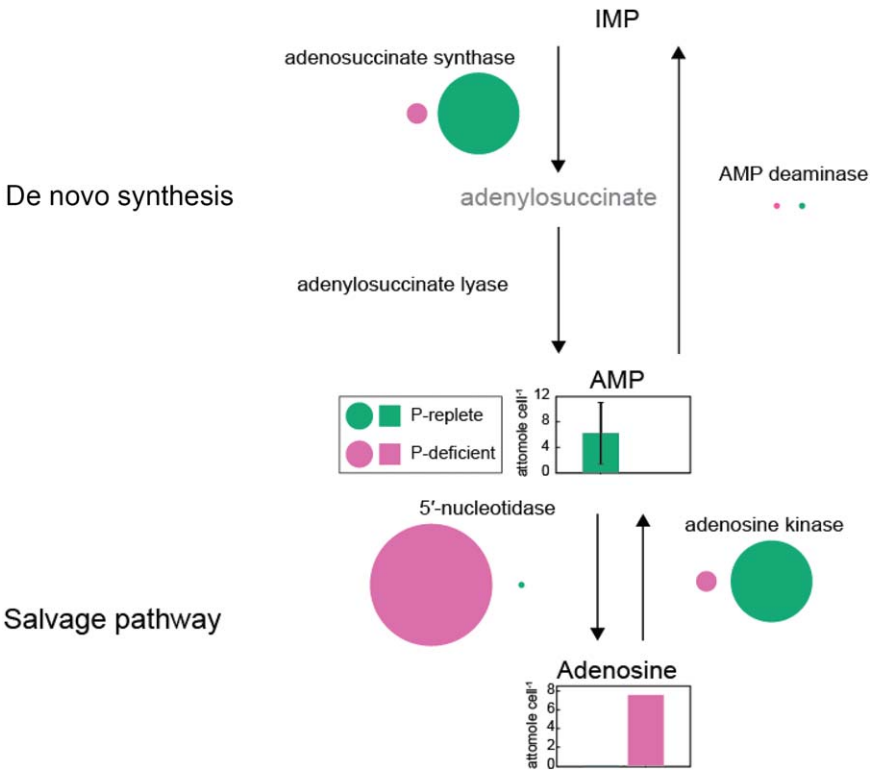

Fig. 3. Relationship between abundance patterns of metabolites and transcripts for a model purine in *T. pseudonana*. Both the de novo synthesis of purines and the salvage pathways are shown. The bar graphs show the metabolite concentrations, relative to an external standard curve and averaged ($n = 8$) across the treatments in amol cell^{-1}; the error bars represent one standard error and are too small to be seen for adenosine. The circles are scaled to denote the transcripts per million for each gene (Dyhrman et al. 2012). The arrows show biochemical pathways linking metabolites. IMP, inosine 5′-monophosphate; AMP, adenosine 5′-monophosphate.

generated from similar treatments but different experiments, revealed relationships between transcripts and metabolites in the purine and pyrimidine pathways (Supporting Information Table S3; Fig. S2). Multiple genes in the *T. pseudonana* purine metabolic pathway had significantly different numbers of transcripts under P-replete compared to P-deficient conditions (Fig. 3; Supporting Information Fig. S2A; Table S3). One of the most highly expressed genes under P-deficient conditions was a phosphohydrolytic 5′-nucleotidase that cleaves phosphate from NMPs to generate the nucleosides. In addition, there were significantly higher numbers of transcripts under P-replete conditions for an adenosuccinate synthase, which catalyzes the conversion of IMP to AMP, and adenosine kinase, which controls production of AMP from adenine (Fig. 3). These patterns suggest that diatoms transcriptionally control nucleotide production under P-replete conditions through the de novo biosynthesis and salvage pathways, and scavenge P from nucleotides under P-deficient conditions.

Nucleotide concentrations in other phytoplankton are affected by P deficiency

We examined the generality of our observations in other eukaryotic phytoplankton by quantifying AMP and adenosine in cultures of *M. pusilla* and *A. anophagefferens* under P-replete and P-deficient conditions (Table 2; Fig. 4). Similar to *T. pseudonana*, the relative concentrations of AMP in *A. anophagefferens* and *M. pusilla* increased under P-replete conditions, while adenosine content increased under P-deficient conditions. Both species upregulate a 5′-nucleotidase gene (Wurch et al. 2011b; Whitney and Lomas 2016) under P deficiency, parallel to the response seen in *T. pseudonana*. In *A. anophagefferens*, the 5′-nucleotidase protein product is also up regulated (Wurch et al. 2011a). In cultures of *M. pusilla*, a cosmopolitan prasinophyte, we observed the same shifts in AMP and adenosine but over a narrower range, suggesting either intrinsic variability in the magnitude of the metabolite restructuring between taxa or variability as a function of relative levels of P deficiency. In summary, despite unavoidable variability in culture conditions across laboratories, P deficiency consistently resulted in a relative decrease in AMP, an increase in adenosine, and an increase in transcripts for a 5′-nucleotidase that could dephosphorylate AMP to produce adenosine.

Liberation of P from NMP dephosphorylation provides a significant quantity of P under P deficiency

Although critical to central metabolism, nucleotide-bound P has typically been viewed as an insignificant component of cellular P relative to P-containing biopolymers

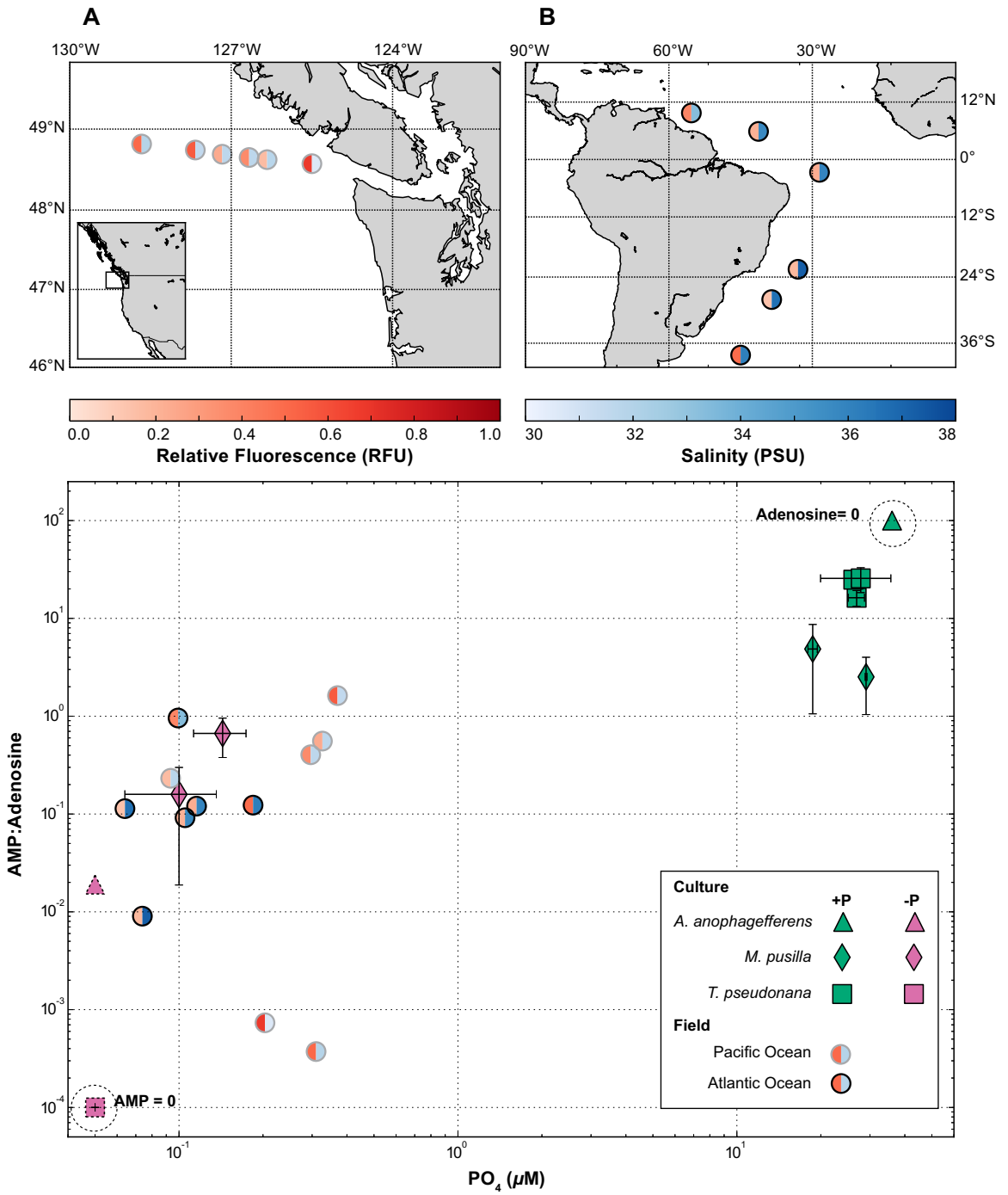

Fig. 4. A comparison of AMP to adenosine ratios from cultures and field sites as a function of the phosphate concentration. (**A**) Field sample locations (gray-outlined circles) collected on 1.6-μm GF/A filters from 5 m depth in the Pacific Ocean. Half of each circle shows the salinity (practical salinity units (PSU): right) and the relative fluorescence (RFU: left), as measured during the downward CTD cast at 5 m. The scales are provided for each measurement in the colorbars. (**B**) Field sample locations (black-outlined circles) collected on 0.7-μm GF/F filters from 5 m depth in the Atlantic Ocean. Same colors as in (**A**). (**C**) AMP to adenosine ratios in field (circles) and culture experiments for *A. anophagefferens* (triangles), *M. pusilla* (diamonds), and *T. pseudonana* (squares) grown under P-replete (green) and P-deficient (pink) conditions. Dashed outlines indicate estimated phosphate concentrations at the method detection limit. A log–log scale is presented to allow all data to be visualized appropriately on one figure. Where available, the mean and one standard deviation of biological replicates at a time-point are presented. Zero concentration values for adenosine and AMP are highlighted.

Table 2. Ratios of AMP to adenosine in all datasets, calculated as moles AMP divided by moles adenosine.

		P treatment	AMP: adenosine range	Mean (± SD)
Cultures	*T. pseudonana*	P-replete	14–32	23 (±6.5)
				n=5
		P-deficient	0	0
				n=6
	M. pusilla	P-replete	1.5–8.8	3.9 (±3.1)
				n=5
		P-deficient	0–1	0.25 (±0.39)
				n=6
	A. anophagefferens	P-replete	∞ (adenosine b.d.)	n/a
		P-deficient	0.019	n/a
Field	Atlantic Ocean*	0.06–0.18 μM	0.01–0.96	0.26 (±0.39)
				n=6
	Pacific Ocean*	0.09–0.37 μM	0.0–1.6	0.47 (±0.61)
				n=6

* The range of dissolved inorganic P concentrations across stations.
b.d., below detection. n/a, not applicable.

such as nucleic acids. If we assume that P is liberated by NMP de-phosphorylation only once within a growth cycle, de-phosphorylation of the observed NMPs liberates ~ 0.08–0.4% of total cellular P (depending on P cell quota; Supporting Information Calculation S2). However, we posit that the flux through a minimal standing concentration of NMPs will need to be high to maintain P homeostasis in P-deficient cells, thus liberating P many times over a growth cycle. We calculate the total amount of P moving through this cycle by first defining the amount of P needed to replicate cell biomass with the observed doubling time (23 days). If we use 0.67 fmol P as our estimate for P cellular quota (Supporting Information Calculation S2), a cell must assimilate 0.02 fmol P day^{-1} to acquire the necessary P. In comparison, the empirical relationship presented in Perry (1976) estimates that P-deficient diatoms assimilate P at a rate of 0.2 fmol day^{-1}. If we conservatively assume no recycling of nucleic acids, the difference between the assimilation rate predicted by Perry (1976) and the minimal assimilation rate calculated here represents the amount of phosphate liberated through this pathway, or (0.2–0.02 fmol) day^{-1} * 23 days = 4 fmol P. We examined the sensitivity of this calculation to growth rate as well as cellular P quota. For the higher cell quota of 2 fmol P and the observed growth rate, the amount of P available would be 2.5 fmol P. Using a higher growth rate (doubling time = 10 days; Dyhrman et al. 2012), the amount of P available would 3 fmol P, assuming the lower P-deficient cell P quota. Only when we combine the higher cell quota with the higher growth rate do we see negligible liberation of P via this mechanism. Given the uncertainties in P-deficient cell quotas and growth rates for P-deficient cells, we estimate that the total P released through rapid NMP dephosphorylation could be the same order of magnitude as the structural P-sparing strategies of lipid substitution (3 fmol; Martin et al. 2011).

Field AMP and adenosine concentrations are similar to laboratory observations for P deficiency

If this is a widespread adaptation to P deficiency in the eukaryotic phytoplankton, then the nucleotide to nucleoside ratio should be low in oligotrophic (low P) environments when eukaryotic phytoplankton are present. We quantified adenosine and AMP using targeted metabolomics in particulate samples collected from 5-m depth in the Atlantic and Pacific Oceans. We then compared AMP to adenosine ratios in field and culture samples as a function of inorganic P concentrations (Fig. 4). In the *T. pseudonana* culture, AMP: adenosine is representative of the shift observed in all nucleotides between the two P conditions. In the field, this ratio is a more tractable measurement than the adenylate charge (ATP + ½ ADP)/(ATP + ADP + AMP) due to the challenge of quenching metabolism quickly enough (within ~ 30 s) to accurately preserve this intracellular ratio (Villas-Boas and Bruheim 2007). Sample filters contained eukaryotes such as diatoms, haptophytes, dinoflagellates, and picoeukaryotes, as well as cyanobacteria and particle-associated bacteria. Even with this increase in microbial diversity in filter samples, we observed AMP-to-adenosine ratios that were quite similar to those observed for our laboratory cultures under P-deficient conditions. Higher field AMP: adenosine values could be due to many factors, including species-derived variability in AMP: adenosine and broad differences in nutrient distributions. Indeed, the highest ratio in the Atlantic Ocean was sampled in the Amazon River plume, which was characterized by high

nutrients, low salinities and high surface chlorophyll fluorescence relative to other sampling sites (Fig. 4). Further work over a range of P environments would help confirm the consistency of the AMP to adenosine ratios as a function of exogenous P concentration or physiological metrics of P deficiency.

Discussion

The combination of transcripts and metabolites studied here point to a new view of P allocation within P-deficient eukaryotic phytoplankton—specifically, that NMPs serve as a dynamic and flexible pool of P for critical energy balance and P homeostasis. We observed uniformly depleted concentrations of NMPs, relative to nucleosides, under P-deficient growth in laboratory cultures of three model phytoplankton. These metabolic shifts appear to be transcriptionally controlled, and the results imply that nucleotides are critical to P homeostasis. Dyhrman et al. (2012) previously attributed the strong pattern of 5′-nucleotidase induction in *T. pseudonana* to the utilization of exogenous DOP. However, the metabolite profiles in this study suggest that the 5′-nucleotidase is acting on intracellular substrates, at least in part. The prevalence of this metabolic shift is further supported by previous studies in marine eukaryotic phytoplankton, where P-deficient conditions were associated with the induction of transcripts and proteins encoding 5′-nucleotidases (Wurch et al. 2011*a*,*b*; Dyhrman et al. 2012; Forster et al. 2014; Whitney and Lomas 2016) as well as enzyme activities with an affinity for nucleotides (Dyhrman and Palenik, 2003; Xu et al. 2013), and enzymes of the purine and pyrimidine pathways (Yang et al. 2014; Feng et al. 2015). Given that variations in physiology can occur between experiments with the same species, the degree of synergy in these disparate data types from separate experiments is striking, and may underscore that phosphate scavenging from NMPs is not a transient response, but one that is a strong and sustained reflection of a low P environment.

The P-modulated changes in the pyrimidine and purine pathways observed herein may be present even more broadly in microbial eukaryotes, as the accumulation of nucleosides was also observed in studies with yeast, where P-deficient growth led to higher cell-normalized concentrations of adenosine, inosine, and other nucleosides (Boer et al. 2010; Ljungdahl and Daignan-Fornier 2012). Further, a nucleotidase that scavenges the phosphate group from NMPs derived from RNA degradation is central to yeast's survival under P deficiency (Xu et al. 2013). We calculated that movement of P through a vanishingly small NMP pool could provide a quantitatively significant source of P to prioritize the most critical cellular processes. Indeed, the conversion between ADP and ATP is the central energy currency of the cell and these reactions must be maintained, even in the face of P deficiency. Studies in yeast, a model eukaryote, show that ATP levels are affected by P deficiency, but are never fully depleted (Boer et al. 2010). In summary, P deficiency induces shifts between NMPs and nucleosides among disparate eukaryotic taxa, suggesting that scavenging of P from NMPs may be common and an evolutionarily conserved feature of P homeostasis in microbial eukaryotes. Although 5′-nucleotidases in marine cyanobacteria and heterotrophic bacteria are not generally upregulated as a function of P deficiency (Ammerman and Azam 1985; Tammienen 1989), recent metabolic modeling work implicates P recycling mechanisms such as this in the response of the cyanobacterium *Prochlorococcus marinus* to P deficiency (Casey et al. 2016).

The environmental shift in the particulate nucleotide to nucleoside ratios is likely to concomitantly impact dissolved organic matter, as some fraction of these and other cellular metabolites will be exuded by the cell during growth, viral lysis or microzooplankton grazing (Moran et al. 2016). Dissolved concentrations of triphosphate nucleotides (e.g., ATP) have been measured in seawater for decades (Azam and Hodson 1977; Björkman and Karl 2001) as a small fraction of the DOP standing stock (Björkman et al. 2000). In contrast, few measurements of AMP are available (Karl and Holm-Hansen 1978) and thus its contribution to DOP is unknown. In general, nucleotides (mono-, di-, and tri-phosphate) are highly bioavailable to both marine prokaryotic and eukaryotic microbes, particularly when phosphate concentrations are low (Azam and Hodson 1977; Nawrocki and Karl 1989; Björkman and Karl 1994). The metabolomics data presented here suggests, however, that these highly labile molecules are depleted in eukaryotic phytoplankton under low P and thus would not enter the dissolved organic matter pool to an appreciable extent.

Low-P environments in both the Atlantic and the Pacific exhibit similar AMP-to-adenosine ratios to those in culture, suggesting that scavenging of nucleotide phosphate is occurring in eukaryotic phytoplankton field populations. Incubation studies are needed to assess the temporal sensitivity of this ratio to P concentrations, the flux of P through NMPs, and the reversibility of low AMP to adenosine ratios under P addition. Despite these uncertainties, the similarity of field ratios with those in our culture experiments indicates that NMPs may play a more important role in environmental P homeostasis in marine eukaryotic phytoplankton than was previously appreciated. When P is low, cells need a flexible storage pool from which to distribute P quickly among cellular phosphorylation processes such as energy balance and signal transduction. NMPs could provide such a pool of P, allowing eukaryotic cells to use the NMP pool as their wallet, living from paycheck to paycheck, redistributing their P currency as needed to maintain cellular processes.

References

Altschul, S. F., T. L. Madden, A. A. Schäffer, J. Zhang, Z. Zhang, W. Miller, and D. J. Lipman. 1997. Gapped BLAST and PSI-BLAST: A new generation of protein database search programs. Nucleic Acids Res. **25**: 3389–3402. doi: 10.1093/nar/25.17.3389

Ammerman, J. W., and F. Azam. 1985. Bacterial 5′-nucleotidase in aquatic ecosystems: A novel mechanism of phosphorus regeneration. Science **227**: 1338–1340. doi: 10.1126/science.227.4692.1338

Armbrust, E. V., and others. 2004. The genome of the diatom Thalassiosira pseudonana: Ecology, evolution, and metabolism. Science **306**: 79–86. doi:10.1126/science.1101156

Azam, F., and R. E. Hodson. 1977. Dissolved ATP in the sea and its utilisation by marine bacteria. Nature **267**: 696–698. doi:10.1038/267696a0

Björkman, K. M., and D. M. Karl. 1994. Bioavailability of inorganic and organic phosphorus compounds to natural assemblages of microorganisms in Hawaiian coastal waters. Mar. Ecol. Prog. Ser. **111**: 265–273. doi:10.3354/meps111265

Björkman, K. M., A. L. Thomson-Bulldis, and D. M. Karl. 2000. Phosphorus dynamics in the North Pacific subtropical gyre. Aquat. Microb. Ecol. **22**: 185–198. doi: 10.3354/ame022185

Björkman, K. M., and D. M. Karl. 2001. A novel method for the measurement of dissolved adenosine and guanosine triphosphate in aquatic habitats: Applications to microbial ecology. J. Microbiol. Methods **47**: 159–167. doi: 10.1016/S0167-7012(01)00301-3

Boer, V. M., C. A. Crutchfield, P. H. Bradley, D. Botstein, and J. D. Rabinowitz. 2010. Growth-limiting intracellular metabolites in yeast growing under diverse nutrient limitations. Mol. Biol. Cell **21**: 198–211. doi:10.1091/mbc.E09-07-0597

Bromke, M. A., P. Giavalisco, L. Willmitzer, and H. Hesse. 2013. Metabolic analysis of adaptation to short-term changes in culture conditions of the marine diatom *Thalassiosira pseudonana*. PLoS One **8**: e67340. doi:10.1371/journal.pone.0067340

Casey, J. R., A. Mardinoglu, J. Nielsen, and D. M. Karl. 2016. Adaptive evolution of phosphorus metabolism in *Prochlorococcus*. mSystems **1**: e00065–00016. doi:10.1128/mSystems.00065-16

Dettmer, K., P. A. Aronov, and B. D Hammock. 2007. Mass spectrometry-based metabolomics. Mass Spectrom. Rev. **26**: 51–78. doi:10.1002/mas.20108

Dittmar, T., B. Koch, N. Hertkorn, and G. Kattner. 2008. A simple and efficient method for the solid-phase extraction of dissolved organic matter (SPE-DOM) from seawater. Limnol. Oceanogr. Methods **6**: 230–235. doi: 10.4319/lom.2008.6.230

Dyhrman, S. T. 2016. Nutrients and their acquisition: Phosphorus physiology in microalgae, p. 155–183. *In* J. Beardall, M. Borowitzka, and J. Raven [eds.], Developments in applied phycology. Springer.

Dyhrman, S. T., and B. Palenik. 2003. Characterization of ectoenzyme activity and phosphate-regulated proteins in the coccolithophorid *Emiliana huxleyi*. J. Plankton Res. **25**: 1215–1225. doi:10.1093/plankt/fbg086

Dyhrman, S. T., and others. 2012. The transcriptome and proteome of the diatom *Thalassiosira pseudonana* reveal a diverse phosphorus stress response. PLoS One **7**: e33768. doi:10.1371/journal.pone.0033768

Feng, T. -Y., and others. 2015. Examination of metabolic responses to phosphorus limitation via proteomic analyses in the marine diatom *Phaeodactylum tricornutum*. Sci. Rep. **5**: 10373. doi:10.1038/srep10373

Forster, R. R., and others. 2014. Extensive liquid meltwater storage in firn within the Greenland ice sheet. Nat. Geosci. **7**: 95–98.

Hockin, N. L., T. Mock, F. Mulholland, S. Kopriva, and G. Malin. 2012. The response of diatom central carbon metabolism to nitrogen starvation is different from that of green algae and higher plants. Plant Physiol. **158**: 299–312. doi:10.1104/pp.111.184333

Johnson, W. M., M. C. Kido Soule, and E. B. Kujawinski. 2016. Evidence for quorum sensing and differential metabolite production in response to DMSP by a marine heterotrophic bacterium. ISME J. **10**: 2304–2316. doi:10.1038/ismej.2016.6

Karl, D. M. 2014. Microbially mediated transformations of phosphorus in the sea: New views of an old cycle. Ann. Rev. Mar. Sci. **6**: 279–337. doi:10.1146/annurev-marine-010213-135046

Karl, D. M., and O. Holm-Hansen. 1978. Methodology and measurement of adenylate energy charge ratios in environmental samples. Mar. Biol. **48**: 185–197. doi:10.1007/BF00395018

Kido Soule, M. C., K. Longnecker, W. M. Johnson, and E. B. Kujawinski. 2015. Environmental metabolomics: Analytical strategies. Mar. Chem. **177**: 374–387. doi:10.1016/j.marchem.2015.06.029

Ljungdahl, P. O., and B. Daignan-Fornier. 2012. Regulation of amino acid, nucleotide, and phosphate metabolism in *Saccharomyces cerevisiae*. Genetics **190**: 885–929. doi: 10.1534/genetics.111.133306

Luo, W., and C. Brouwer. 2013. Pathview: An R/Bioconductor package for pathway-based data integration and visualization. Bioinformatics **29**: 1830–1831. doi:10.1093/bioinformatics/btt285

Martin, P., B. A. S. Van Mooy, A. Heithoff, and S. T. Dyhrman. 2011. Phosphorus supply drives rapid turnover of membrane phospholipids in the diatom *Thalassiosira pseudonana*. ISME J. **5**: 1057–1060. doi:10.1038/ismej.2010.192

Montagnes, D. J. S., J. A. Berges, P. J. Harrison, and F. J. R. Taylor. 1994. Estimating carbon, nitrogen, protein, and chlorophyll *a* from volume in marine phytoplankton. Limnol. Oceanogr. **39**: 1044–1060. doi:10.4319/lo.1994.39.5.1044

Moran, M. A., and others. 2016. Deciphering ocean carbon in a changing world. Proc. Natl. Acad. Sci. USA. **113**: 3143–3151. doi:10.1073/pnas.1514645113

Nawrocki, M. P., and D. M. Karl. 1989. Dissolved ATP turnover in the Bransfield Strait, Antarctica during a spring bloom. Mar. Ecol. Prog. Ser. **57**: 35–44. doi:10.3354/meps057035

Patti, G. J., O. Yanes, and G. Siuzdak. 2012. Metabolomics: The apogee of the omics trilogy. Nat. Rev. Mol. Cell Biol. **13**: 263–269. doi:10.1038/nrm3314

Perry, M. J. 1976. Phosphate utilization by an oceanic diatom in phosphorus-limited chemostat culture and in the oligotrophic waters of the central North Pacific. Limnol. Oceanogr. **21**: 88–107. doi:10.4319/lo.1976.21.1.0088

Poulson-Ellestad, K. L., C. M. Jones, J. Roy, M. R. Viant, F. M. Fernández, J. Kubanek, and B. L. Nunn. 2014. Metabolomics and proteomics reveal impacts of chemically mediated competition on marine plankton. Proc. Natl. Acad. Sci. USA **111**: 9009–9014. doi:10.1073/pnas.140213011

Rabinowitz, J. D., and E. Kimball. 2007. Acidic acetonitrile for cellular metabolome extraction from *Escherichia coli*. Anal. Chem. **79**: 6167–6173. doi:10.1021/ac070470c

Storey, J. D., and R. Tibshirani. 2003. Statistical significance for genomewide studies. Proc. Natl. Acad. Sci. USA **100**: 9440–9445. doi:10.1073/pnas.1530509100

Tammienen, T. 1989. Dissolved organic phosphorus regeneration by bacterioplankton: 5′-nucleotidase activity and subsequent phosphate uptake in a mesocosm enrichment experiment. Mar. Ecol. Prog. Ser. **58**: 89–100. doi:10.3354/meps058089

Van Mooy, B. A. S., and others. 2009. Phytoplankton in the ocean use non-phosphorus lipids in response to phosphorus scarcity. Nature **458**: 69–72. doi:10.1038/nature07659

Villas-Boas, S. G., and P. Bruheim. 2007. Cold glycerol-saline: The promising quenching solution for accurate intracellular metabolite analysis of microbial cells. Anal. Biochem. **370**: 87–97. doi:10.1016/j.ab.2007.06.028

Whitney, L. P., and M. W. Lomas. 2016. Growth on ATP elicits a P-stress response in the picoeukaryote *Micromonas pusilla*. PLoS One **11**: e0155158. doi:10.1371/journal.pone.0155158

Wu, Z., B. D. Jenkins, T. A. Rynearson, S. T. Dyhrman, M. A. Saito, M. Mercier, and L. P. Whitney. 2010. Empirical bayes analysis of sequencing-based transcriptional profiling without replicates. BMC Bioinform **11**: 564. doi:10.1186/1471-2105-11-564

Wurch, L. L., E. M. Bertrand, M. A. Saito, B. A. S. Van Mooy, and S. T. Dyhrman 2011a. Proteome changes driven by phosphorus deficiency and recovery in the brown tide-forming alga *Aureococcus anophagefferens*. PLoS One **6**: e28949. doi:10.1371/journal.pone.0028949

Wurch, L. L., S. T. Haley, E. D. Orchard, C. J. Gobler, and S. T. Dyhrman. 2011b. Nutrient-regulated transcriptional response in the brown tide-forming alga *Aureococcus anophagefferens*. Environ. Microbiol. **13**: 468–481. doi:10.1111/j.1462-2920.2010.02351.x

Xu, Y. -F., and others. 2013. Nucleotide degradation and ribose salvage in yeast. Mol. Syst. Biol. **9**: 665. doi:10.1038/msb.2013.21

Yang, Z. -K., J. -W. Zheng, Y. -F. Niu, W. -D. Yang, J. -S. Liu, and H. -Y. Li. 2014. Systems-level analysis of the metabolic responses of the diatom *Phaeodactylum tricornutum* to phosphorus stress. Environ. Microbiol. **16**: 1793–1807. doi:10.1111/1462-2920.12411

Acknowledgments

We thank C. Breier, G. Swarr, E. Melamund, and G. Hennon for assistance with laboratory work and data analysis. We thank J. Jennings (Oregon State Univ.) and the Armbrust laboratory (Univ. of Washington) for the Atlantic and Pacific inorganic P concentrations, respectively. We thank M. Kido Soule and the WHOI FT-MS Users' Facility for metabolomics analysis. We thank the scientific parties, captains and crews of the R/V *Knorr* and the R/V *Thomas Thompson* for assistance in acquiring the Atlantic and Pacific field samples, respectively. The cruises were funded by the National Science Foundation (Atlantic Ocean: OCE-1154320 to EBK and KL; Pacific Ocean: OCE-1205233 to EV Armbrust). This research was funded by the Gordon and Betty Moore Foundation (Grant 3304 to EBK), the Simons Foundation (SCOPE award ID 329108 to STD), and the National Science Foundation Chemical and Biological Oceanography Programs (OCE-01316036 and OCE-0723667 to STD). HA was supported by a WHOI Ocean Life Institute Fellowship and WMJ was supported by a National Defense Science and Engineering Fellowship.

Submitted 06 September 2016
Revised 02 April 2017
Accepted 10 May 2017